

Growth and structural characterization of Tutton salt mixed of Co and Ni

<http://dx.doi.org/10.1590/0370-44672020760009>

Rodolfo Rocha Vieira Leocádio^{1,3}

<https://orcid.org/0000-0002-0567-3031>

Genivaldo Júlio Perpétuo^{1,4}

<https://orcid.org/0000-0002-3697-7679>

Carlos Joel Franco^{2,5}

<https://orcid.org/0000-0002-1920-2353>

Adriano Corrêa Batista^{1,6}

<https://orcid.org/0000-0002-3515-7281>

¹Universidade Federal de Ouro Preto – UFOP, Universidade Estadual de Minas Gerais – UEMG, REDEMAT - Rede Temática em Engenharia de Materiais, Ouro Preto - Minas Gerais - Brasil.

²Universidade Federal de Ouro Preto - UFOP, Instituto de Ciências Exatas e Biológicas, Ouro Preto - Minas Gerais - Brasil.

E-mails: ³rodolfo.leocadio@ufop.edu.br,

⁴perpetuo@ufop.edu.br, ⁵cjoelfra@ufop.edu.br,

⁶adrianocorrea77@gmail.com

Abstract

The family of crystals known as Tutton's salts plays a significant role in physics and chemistry; because they are used in phase transition studies and to define models applied to materials. The importance of salts in material engineering is recent, as in applications in adiabatic degaussing refrigerators and solid-state anodes. Studies of the $(\text{NH}_4)_2\text{Ni}(\text{SO}_4)_2 \cdot 6\text{H}_2\text{O}$ and $(\text{NH}_4)_2\text{Co}(\text{SO}_4)_2 \cdot 6\text{H}_2\text{O}$ are widely found in literature but do not occur for the mixture of both. In this research, we studied mixed crystals of the general chemical formula $(\text{NH}_4)_2\text{Ni}_x\text{Co}_{(1-x)}(\text{SO}_4)_2 \cdot 6\text{H}_2\text{O}$ with x ranging from 0 to 1, utilizing $x = 0.7$. The objective is to study the modifications caused owing to the ion's weighted composition in the formation of the solid solution and compare it with the pure salts. For this, the growth of these crystals is discussed based on ICP-OES results and optical microscopy concerning the crystal growth theory. The discussion also relates the Raman spectra of the salts with molecular changes according to structured group theory, qualitatively characterizing its crystalline structure. Finally, a Single-crystal X-ray study solves and confirms the structure of pure salts and mixed salt, quantitatively characterizing their crystal structure.

Keywords: Tutton's salts, ICP-OES, optical microscopy, Raman, single-crystal X-ray, and crystalline structure.

1. Introduction

Molecular crystals known as Tutton's Salts have the chemical formula $A_2M(\text{EO}_4)_2 \cdot 6\text{H}_2\text{O}$ with $A = \text{K}^+, \text{NH}_4^+, \text{Rb}^+, \text{Cs}^+$; $M = \text{Co}^{2+}, \text{Ni}^{2+}, \text{Zn}^{2+}, \text{Mn}^{2+}, \text{Mg}^{2+}, \text{Fe}^{2+}, \text{Cu}^{2+}, \text{V}^{2+}, \text{Cd}^{2+}$; and $E = \text{S}^{6+}, \text{Se}^{6+}$ (Marinova *et al.*, 2009; Georgiev *et al.*, 2010). These materials display dielectric characteristics, anisotropy, high purity, diamagnetic or paramagnetic ordering, and phase transitions (Lonsdale, 1937; Ganesh *et al.*, 2013). These characteristics justify their importance in physics, chemistry, and materials engineering.

Many of these crystals have applications: as reagents of considerable reliability and spectroscopic standards (Ganesh *et al.*, 2013); in low-temperature nuclear orientation experiments (Bleaney *et al.*, 1954); in dynamic polarization experiments on dielectric solids used in nuclear physics (Atsarkin, 1978); in Nearest-neighbor-interaction model in the

coupled-optical-phonon-mode theory of the infrared dispersion in monoclinic crystals (Ivanovski and Ivanovski, 2010); and high-frequency Electronic Paramagnetic Resonance (EPR) based studies applied to bio-inorganic systems (Reijerse *et al.*, 1998), among others. These applications characterize the importance of these crystals in physics and chemistry.

Some of them are used in technological applications, such as hydrated salt pellets, used to produce a low temperature in refrigerators of adiabatical-demagnetization (Shirron and Mccammon, 2014), and in the elaboration of new materials used in solid-state anodes for solar cells with electrodes of proton conduction (Telli *et al.*, 2002), among others. These applications characterize the importance of these crystals in materials engineering.

It is possible to obtain mixed single-crystals in the form of solid solutions,

such as $(\text{NH}_4)_2\text{Ni}_x\text{Co}_{(1-x)}(\text{SO}_4)_2 \cdot 6\text{H}_2\text{O}$, with x ranging from 0 to 1 (Fei & Straws, 1995), for the family of Tutton's salts. We found Single-crystal X-ray studies and spectroscopic studies for pure $(\text{NH}_4)_2\text{Ni}(\text{SO}_4)_2 \cdot 6\text{H}_2\text{O}$ and $(\text{NH}_4)_2\text{Co}(\text{SO}_4)_2 \cdot 6\text{H}_2\text{O}$ compounds, but scarce is literature for the mixed ones.

Pure salts are isostructural, crystallize in the monoclinic system, belong to the space group $\text{P2}_{1/c}$ (C^5_{2h}), and have twice the formula in the unit cell ($Z = 2$). The structure is also described from distorted octahedra of $[\text{M}(\text{H}_2\text{O})_6]^{2+}$ and tetrahedra of SO_4^{2-} and NH_4^+ , shown in Figure 1 (Li & Li, 2004; Tahirov & Lu, 1994). The cation $M = \text{Ni}$ or Co occupies the octahedron center, and six water molecules occupy your vertices. Only three water molecules are crystallographically independent. These octahedra and tetrahedra interact with each other using hydrogen bonds.

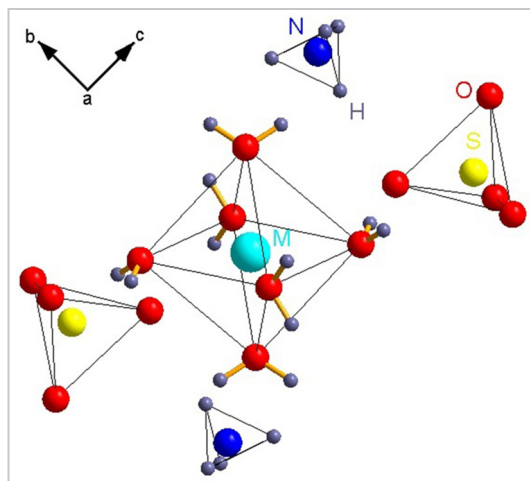


Figure 1 - Structure of the $(\text{NH}_4)_2\text{M}(\text{SO}_4)_2 \cdot 6\text{H}_2\text{O}$ ($\text{M} = \text{Ni}$ or Co). Formulated using Li and Li (2004).

According to Cotton *et al.* (1993), Tahirove & Lu (1994), Cotton *et al.* (1994), and Li & Li (2004), the structure of these salts exhibits a complex network of hydrogen bonds allowing the whole series to be isomorphic. The twelve hydrogen atoms of the group $[\text{M}(\text{H}_2\text{O})_6]^{2+}$ and the four of the NH_4^+ group partici-

pate in hydrogen bonds in the structure. The group theory analysis for the active vibrational modes in Raman predicts 114 ($57 A_g$ and $57 B_g$) vibrational modes: 45 internals, 6 librations, and 6 translations (Barashkov *et al.*, 2000). The objective of this article is to present and discuss the method of crystal growth

and its structure using the techniques of Inductively Coupled Plasma Optical Emission Spectrometry (ICP-OES) characterization, optical microscopy, Raman spectroscopy, and Single-crystal X-ray. This study compares the spectra of the pure salts containing Ni and Co, widely found in literature, to the mixed salt.

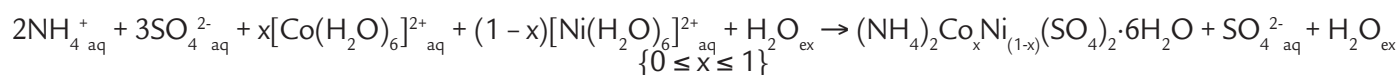
2. Materials and methods

The solvent used for crystal growth was water. The solutes used were the analytical reagents: $\text{NiSO}_4 \cdot 6\text{H}_2\text{O}$ -

Nickel Sulfate (98 %) hexahydrate, $\text{CoSO}_4 \cdot 7\text{H}_2\text{O}$ - Cobalt Sulfate (99%) heptahydrate, $(\text{NH}_4)_2\text{SO}_4$ - Ammo-

onium Sulfate (99 %). The growth process occurs according to the chemical equation 1.

Equation 1 - Chemical equation of mixed salt preparation.



The crystal growth method by isothermal evaporation of the solution in water allows for growing crystals with natural faces and small concentrations of structural defects (Andreea, 1999). The solution was prepared with pre-established quantities of the reagents solubilized in deionized water until it reached a volume of $80 \times 10^{-6} \text{ m}^3$ at a temperature of 343 K, filtered, and placed in the growth oven at a constant temperature and equal to 313 K (± 1) for periods of up to two weeks.

It used Agilent 725 ICP-OES, with 99.996% purity Argon gas for plasma formation. The selected samples were

observed in the Leica DMRX optical microscope and taken to the Raman without any preparation. Only then were they dissolved in $25 \times 10^{-6} \text{ m}^3$ of distilled water, with constant stirring to expedite dissolution.

Used was a Horiba / Jobin-Yvon LABRAM-HR spectrometer with the 632.8 nm line of a helium-neon laser (power of $6 \times 10^{-3} \text{ W}$ applied on the sample surface) as an excitation source, a diffraction grating 600×10^3 slots/m (for all spectrum) and 1800×10^3 slots/m (for better resolution of the low wavenumber region), Peltier-cooled CCD detector, Olympus confocal microscope (100x objective), experimental

resolution of typically $10 \times 10^{-3} \text{ m}^{-1}$ (10 accumulations in 30 s).

Drop-shaped crystals ($\approx 200 \times 10^{-6} \text{ m}$) generated X-ray patterns, collected at a temperature of 293(2) K in the Oxford Diffraction Gemini A Ultra equipped with a CCD detector, using Mo-K α radiation ($\lambda = 0.71073 \times 10^{-10} \text{ m}$). Used WinGX - Version 2014.1 software (Farrugia, 1999) to solve and refine the structure, CrysAlisPro software for data collection and reduction, jointly with the SHELX package (Sheldrick, 2008), and Diamond Version 4.0.1 and Mercury 3.5.1 as a software of graphic design.

3. Results

Single crystals obtained using the growth process are exhibited in Figure 2, with adequate morphology and high purity. Samples 1, 2, and 3 correspond to $(\text{NH}_4)_2\text{Co}(\text{SO}_4)_2 \cdot 6\text{H}_2\text{O}$,

$(\text{NH}_4)_2\text{Ni}(\text{SO}_4)_2 \cdot 6\text{H}_2\text{O}$, and $(\text{NH}_4)_2\text{Co}_{0.3}\text{Ni}_{0.7}(\text{SO}_4)_2 \cdot 6\text{H}_2\text{O}$, respectively. In the study, the adsorption of impurities is insignificant because there was scientific rigor in its preparation.

The size of the crystalline samples is related to the growth time variable, ranging from micron to centimeters scales. Micrographs of the crystals are in Figure 3.

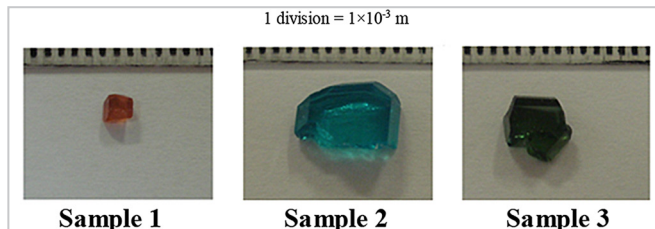


Figure 2 - Photographs of the crystals.

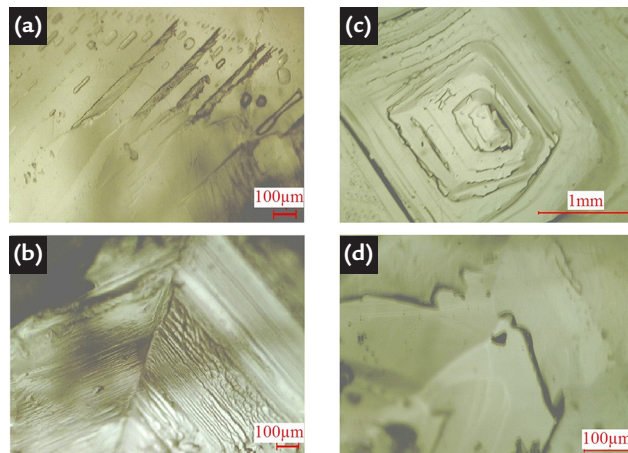


Figure 3 - Increased micrographs a) 80x, b) 80x, c) 40x and d) 200x of the Co-Ni mixed salt.

The results of the ICP-OES analysis with direct quantitative information on the concentration of the

elements (in mg/kg), considering the analytical lines that best fit the model, are presented in Table 1, together with

the theoretical values stoichiometrically calculated according to Lide and Baysinger (2009).

Table 1 - Quantification using ICP-OES.

Elements	Co		Ni		S	
Analytical line ($\times 10^{-6}$ m)	239		217		182	
Unity	mg/kg					
Data type	T ^a	E ^b	T ^a	E ^b	T ^a	E ^b
Sample 1	149111	158335	0	< DL	162271	147345
Sample 2	0	< DL	148594	153698	162363	143284
Sample 3	74578	46188	74274	111191	162310	147262
Detection Limit (DL)	-	1	-	2	-	4

^aTheoretical, ^b Experimental

The result of the Raman analysis is shown in Figure 4. We divide the spectrum between 50 and 4000 cm^{-1} in:

low wavelength region (a) between 50 cm^{-1} and approximately 400 cm^{-1} ; region intermediate (b) between 400 cm^{-1} and

1300 cm^{-1} ; region of high wavenumbers (c) as from 1300 cm^{-1} .

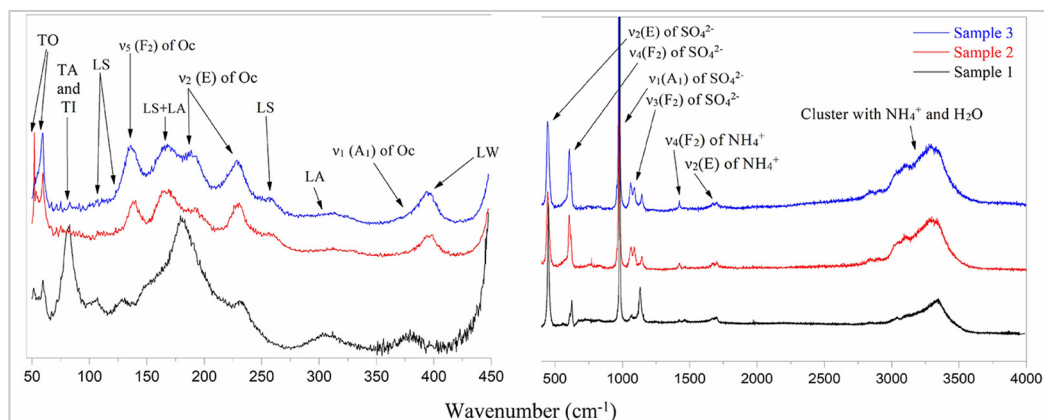


Figure 4 - Raman spectrum.

In region (a), observe an aggregate of overlapping bands that are associated (Barashkov *et al.* 2000): i) to the octahedral complex; ii) to libration modes of

SO_4^{2-} , NH_4^+ and H_2O designated as LS, LA, and LW, respectively; iii) to translation modes of SO_4^{2-} with $[\text{M}(\text{H}_2\text{O})_6]^{2+}$, NH_4^+ with SO_4^{2-} and a mixed character

with contributions from the three ions designated TO, TA and TI, respectively. The wavenumbers describing this region are in Table 2.

Table 2 - Raman spectrum vibrational modes for the region (a).

Modes (cm ⁻¹)	Barashkov <i>et al.</i> (2000)	Sample 1	Sample 2	Sample 3
TO	44-65	51	51	55
		59	58	59
TA and TI	75-100	81	-	-
LS	107-130	107	-	-
		125	-	-
$\nu_3(\text{F}_2)$ of Oc*	139-152	152	137	135
LSA	162-174	-	167	167
$\nu_2(\text{E})$ of Oc*	182-246	180	-	-
		184	192	190
		232	229	228
LS	258-276	-	256	276
LA	295-346	306	308	304
$\nu_1(\text{A}_1)$ of Oc*	363-377	378	380	377
LW	387-398	400	396	395

*Octahedron

In region (b), four bands of the SO_4^{2-} stand out and some low-intensity bands. The low-intensity bands can be associated with libration modes of the H_2O

(Marinova *et al.*, 2009 and, Georgiev *et al.*, 2010). Finally, in region (c), there are several weak bands between 1300 cm⁻¹ and 2700 cm⁻¹ and a cluster between 2700 cm⁻¹

and 4000 cm⁻¹ that correspond mainly to NH_4^+ and H_2O (Dong *et al.*, 2007). The wavenumbers describing these two regions are in Table 3.

Table 3 - Raman spectrum vibrational modes for regions (b) and (c).

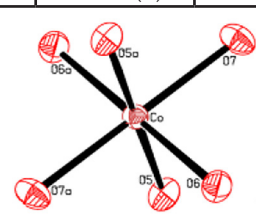
Vibrational modes	SO_4^{2-} (cm ⁻¹)				NH_4^+ (cm ⁻¹)			H_2O (cm ⁻¹)		
	$\nu_1(\text{A}_1)$	$\nu_2(\text{E})$	$\nu_3(\text{F}_2)$	$\nu_4(\text{F}_2)$	$\nu_1(\text{A}_1)$	$\nu_1(\text{A}_1) + \nu_3(\text{F}_2)$	$\nu_3(\text{F}_2)$	$\nu_1(\text{A}_1)$	$\nu_3(\text{B}_2)$	$\nu_3(\text{B}_2)$
Dong <i>et al.</i> (2007)	975	451	1104	612	2878	3032	3040	3248	3468	3628
Sample 1	975	447	1095	605	2845	2907	3023	3099	3238	3340
Sample 2	975	450	1096	607	2877	2900	3030	3098	3259	3331
Sample 3	975	451	1095	607	2833	2932	3017	3084	3283	3353

Single-crystal X-ray study confirms the structure obtained by Li & Li (2004) and Tahirov and Lu (1994)

for pure cobalt and nickel compounds, respectively. The geometric parameters of the metal coordination octahedron

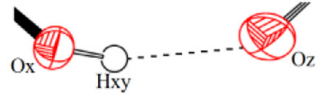
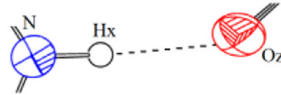
are in Table 4, and the hydrogen bonds and parameters of the mixed salt are in Table 5.

Table 4 - Parameters of bonds of the octahedron.

Bond	O1-M-O2 (°)			WA*	O ₁ -M (Å)			WA*
	Co	Ni	Co-Ni	Co-Ni	Co	Ni	Co-Ni	Co-Ni
O5-M-O5 ^a	180	180	180	180	2.063(1)	2.0341(1)	2.044(1)	2.043(1)
O6-M-O6 ^a	180	180	180	180	2.103(2)	2.0647(1)	2.073(1)	2.076(2)
O7-M-O7 ^a	180	180	180	180	2.103(9)	2.0653(1)	2.0763(9)	2.077(9)
O5-M-O6	88.8(2)	89.70(7)	89.3(9)	89.4(3)				
O5-M-O6 ^a	91.1(8)	90.29(3)	90.6(1)	90.5(8)				
O6-M-O7	88.9(8)	88.41(6)	88.6(1)	88.6(9)				
O6-M-O7 ^a	91.0(2)	91.58(6)	91.3(8)	91.4(3)				
O5-M-O7	89.6(9)	89.36(6)	89.4(7)	89.4(9)				
O5-M-O7 ^a	90.3(1)	90.63(4)	90.5(3)	90.5(1)				

* Weighted Average with 70% Ni and 30% Co

Table 5 - Parameters of hydrogen bonding in the crystals.

Interaction	D-H...A (°)		WA*			H...A (Å)		WA*	Symmetry	
	M =	Co	Ni	Co-Ni	Co-Ni	Co	Ni	Co-Ni		
O5-H5A...O4	175(3)	175(3)	176(3)	175(6)	1.933(3)	1.911(3)	1.894(2)	1.918(6)	1-x, 1-y, 1-z	
O5-H5B...O3	170(3)	170(3)	170(2)	170(6)	2.036(3)	2.033(3)	2.028(2)	2.034(6)	1-x, 0,5+y, 1,5-z	
O6-H6A...O1	171(3)	171(3)	171(3)	171(6)	1.947(2)	1.964(3)	1.914(2)	1.959(5)	1-x, 0,5+y, 1,5-z	
O6-H6B...O2	174(3)	173(3)	173(2)	174(6)	1.971(3)	1.965(3)	1.942(2)	1.967(6)	2-x, 0,5+y, 1,5-z	
O7-H7A...O3	175(3)	165(3)	166(3)	168(6)	2.043(3)	2.018(3)	1.991(3)	2.026(6)	-1+x, y, z	
O7-H7B...O1	175(3)	173(3)	174(2)	174(6)	2.115(3)	2.105(3)	2.060(3)	2.108(6)	x, 0,5-y, 0,5+z	
										
N-HA...O1	154(2)	161(3)	158(2)	159(5)	2.208(3)	2.164(3)	2.130(3)	2.178(6)	1-x, 1-y, 2-z	
N-HB...O3	159(3)	163(3)	159(2)	162(6)	2.204(2)	2.161(3)	2.126(2)	2.174(5)	1-x, 0,5+y, 1,5-z	
N-HC...O4	167(3)	166(3)	165(3)	167(6)	2.133(3)	2.091(3)	2.082(3)	2.104(6)	2-x, 1-y, 2-z	
N-HD...O4	175(2)	178(3)	179(2)	177(5)	1.973(3)	1.990(4)	2.019(3)	1.985(7)	x, y, z	

* Weighted Average with 70% Ni and 30% Co

4. Discussion

The formation of nuclei is the initial stage of crystallization. This step is possible only when kinetic energy barriers for the agglomeration of molecules are overcome (Saito, 1996). These barriers are supersaturation conditions. Evaporation of the solvent at a constant temperature of 313 K increases supersaturation. Increasing the supersaturation increases the velocity of the nucleation. Thus, it forms a sufficient number of smaller nuclei for crystallization. In the isothermal process, nucleation happens when there is the continuous exchange of the solidification-latent heat between the core and the solution, as described in Saito (1996) by the homogeneous nucleation theory.

After the nucleation stage, the crystal goes on to the growth phase. This phase occurs as a successive and periodic ordering of atoms or molecules to form a standard structure, producing the repetition of a unit cell. This process occurs according to the theory of kink formation described in Pimpinelli and Villain (1999), which uses diffusion as its principal mechanism. The diffusion fields are formed, which give rise to surfaces that grow due to the presence of layers associated with defects in the crystal and, in particular, screw dislocations, as described in Pimpinelli & Villain (1999). Figure 3 contains micrographs with the sample surfaces that prove the growth model discussed.

Liquid inclusions present in crystals can be viewed in Figure 3a. Volumes -

where growth units forming the diffusion fields were not indexed, that is - not filled by the solution, cause these inclusions. In Figure 3b, we observe the two-dimensional growth mechanism known as Kink's formation (Pimpinelli & Villain, 1999), and in Figure 3c, the three-dimensional growth mechanism (formation of growth layers). Surface defects such as irregularities and holes are in Figure 3d.

Analyzing the quantities of the chemical elements (Table 1) obtained by the ICP-OES method, the element S has experimental values approximated to the theoretical values in pure and mixed samples. The same is true for Ni and Co elements in the pure salts. In mixed salt, however, we can observe in the experimental result that the quantity of Co is smaller, and that of Ni is higher than predicted in the theoretical model. Therefore, the concentrations of these metals in the crystal differ from the stoichiometric values used for the synthesis.

Thermodynamic models describe the growth process as a binary system because it is always possible to obtain a single solid phase in the entire concentration interval. So, we acquire mixed monocrystals with the form $\text{Co}_{(1-x)}\text{Ni}_x$ for $0 \leq x \leq 1$, producing compounds with the same crystal structure (Pimpinelli & Villain, 1999).

At 343 K, we have the solution in the liquid phase. As the temperature decreases, we have a biphasic region. In this region, the first crystals in the solution

begin to nucleate, coexisting with solid and liquid. Because it is a practical procedure, concentrations are shifted, creating a metastability region until crystals form and solids remain with divergences in their concentrations. Under these conditions, the solid must homogenize through the kink's forming diffusion mechanisms to originate a solid solution. Thus, a balance deviation occurs (displacement of the solidus line), causing the system to assume metastable conditions.

In the negative deviation of the solidus line, there is no tendency for phase separation. At low temperatures, when the thermal energy of atoms becomes smaller, there is a tendency for randomness in the distribution of octahedral molecules. Believed this trend is caused to distortions in the octahedral complexes induced by the Jahn-Teller effect (Cotton *et al.*, 1993).

The experimental values in Table 1 reveal an amount of Co = 30% and Ni = 70% where it should be Co = 50% and Ni = 50%. Crystal growth by the isothermal evaporation of the solution in water gives rise to crystals consisting of a regular solution (unbalanced cooling) that favors $[\text{Ni}(\text{H}_2\text{O})_6]^{2+}$ ions. Therefore, the growth method must consider the metastability conditions to obtain the entire concentration range.

The mixed salt spectrum is the stoichiometric sum containing the pure salt spectra. Any different value within the concentration range converges to

the same result, as we will always have intermediate values.

In region (b), according to Georgiev *et al.* (2010), the band corresponding to $\nu_1(A1)$ is single, $\nu_2(E)$ is double, $\nu_3(F2)$ and $\nu_4(F2)$ are triple. This description is consistent with Table 3, but no changes in the pure salt bands occurred compared to the mixed salt spectrum. Therefore, vibrational modes remain degenerate even with changes in composition.

In region (c), NH_4^+ exhibits vibrational modes equivalent to SO_4^{2-} (Georgiev *et al.*, 2010, Frost *et al.*, 2011). $\nu_1(A1)$ and $\nu_3(F2)$ of NH_4^+ are in a cluster with $\nu_1(A1)$ and $\nu_3(B2)$ of H_2O . In the spectrum, it is not possible to associate the $\nu_2(A1)$ bands of the H_2O , expected at 1595 cm^{-1} (Best *et al.*, 2006). The intensity versus shift Raman for the $\nu_2(E)$ and $\nu_4(F2)$ of the NH_4^+ vibrational modes is low, causing the noise. Even so, the spectrum presents, for the vibrational mode $\nu_4(F2)$, a band at 1424 cm^{-1} , above the wave number reported by Georgiev *et al.* (2010), 1400 cm^{-1} . For the $\nu_2(E)$ vibrational mode, the spectrum has two bands, whose average is 1685 cm^{-1} , subtly above the wave number reported by Marinova *et al.* (2009), 1680 cm^{-1} . The displacement noted for the molecule in a solid may be misunderstood due to the low intensity. Therefore, $\nu_4(F2)$ and $\nu_2(E)$ continue to feature one and two bands, respectively. Even with changes in composition, they remain degenerate.

The details of the vibrational modes related to the cluster are presented in Table 3, as performed by Dong *et al.* (2007). The values agree well with experimental NH_4^+ data but are above the wavenumbers reported for a molecule in solution (Dong *et al.*, 2007). This difference occurs through the interaction with their neighbors in this solid. Therefore, these vibrational modes are also not significantly influenced by changes in composition.

The positions of the SO_4^{2-} ions in the unit cell are identical, and their geometry shows slight distortions from tetrahedral geometry. The same is true for NH_4^+ , whose hydrogen bonds are moderate. The anharmonic force fields and the low polarizability of NH_4^+ ions cause the width increase and the low intensity of the bands. The same does not happen with the corresponding SO_4^{2-} ions, although both belong to the same point group and occupy sites with identical symmetry. Thus, it's possible to infer that SO_4^{2-} is spinning freely in the structure, which is not the case with NH_4^+ (Rajagopal &

Aruldas, 1989).

The wavenumbers of the SO_4^{2-} and NH_4^+ vibrational modes in Tutton's salt structure accompany the predictions of group theory (Nakamoto, 1986), having symmetry described by the point group Td. That is, SO_4^{2-} and NH_4^+ are present in the salt structure with the geometrical form of a tetrahedron whose vibrational modes are not sensitive to changes in composition in the solid solution.

The values corresponding to H_2O do not agree with those reports by Dong *et al.* (2007) but are in the same region. The coordination of the molecule in the crystal causes the deviation and shifts the bands to the left. The difference in the displacement of vibrational modes is related to the M–O coordination distances, which polarize the water molecules to strengthen the bonds. As the ionic radius of M^{2+} decreases, their interaction with water increases. Thus, the spectrum of the solid solution exhibits larger displacements than the others.

The wavenumbers of the H_2O vibrational modes in the Tutton salt structure accompany the predictions of group theory (Nakamoto, 1986) with symmetry described by the point group C_{2v} . However, the compound is coordinated, and therefore it does not only address the properties of the point group for free molecules.

In region (a), the active vibrational modes in Raman of the octahedral complex are $\nu_1(A1)$, $\nu_2(E)$, and $\nu_5(F2)$ (Nakamoto, 1986). The vibrational modes of sample 1 present modifications caused by the Jahn-Teller effect, which is more pronounced in this sample. $[M(H_2O)_6]^{2+}$ ions are influenced by composition changes due to octahedron shape distortions (Barashkov *et al.*, 2000). According to Table 2, the pseudo-octahedral vibrational modes accompany the predictions of group theory (Nakamoto, 1986), with symmetry described by the point group Oh. That is, $[M(H_2O)_6]^{2+}$ is present in the salt structure with the geometric shape of a slightly distorted octahedron. Wyckoff's position is 2a and occupies a high symmetry site, so his local symmetry is C_1 .

Libration modes arise from rotations about their three main axes constrained by interactions with their neighboring atoms (Nakamoto, 1986, Best *et al.*, 2006). The bands corresponding to LS and LS+LA have modifications, and the bands LW and LA are unchanged. Octahedron distortion affects its nearest

neighbors, causing changes in libration modes of SO_4^{2-} and slightly affecting NH_4^+ . Therefore, the wavenumbers of the libration modes of SO_4^{2-} , NH_4^+ , and H_2O in Tutton's salt structure accompany the predictions of group theory, its position being Wyckoff 4e and occupying a low symmetry site. Therefore, its local symmetry is C_1 .

Translational modes shift the molecule center of mass into one of three coordinates of 3-D space. These arise from the unit cell containing the octahedron, SO_4^{2-} , and NH_4^+ vibrating as a coupling of molecules (Vandenabeele, 2013). The Jahn-Teller effect causes modifications in sample 1, affecting the interaction of the octahedral complex with SO_4^{2-} , which affects its interaction with NH_4^+ (change in TA), and reflects in TI, inducing its modification. The wavenumbers of the translation modes in Tutton's salt structure accompany the predictions of the group theory (Nakamoto, 1986), confirming that the studied molecules interact with each other and are the most affected by solid solution formation.

Ni and Co atoms present a static occupational disorder in which two different types of metals can alternately occupy the same site (mixed crystals). The refined probabilities in Single-crystal X-ray are 69.3(3)% and 30.3(1)% for Ni and Co, respectively.

Table 4 has the geometric parameters for the octahedral complex. We realize that these have the effect of Jahn-Teller (Cotton *et al.*, 1993), caused by the unfolding of the orbitals d in a degenerated state that suffers this kind of distortion to reduce its symmetry and remove degeneration. As expected, the mixed salt results are the weighted average of pure crystals.

Notice the slight differences in the bonds and the angles O – H of the H_2O . These distortions can be caused by interaction with the neighborhood because the molecule coordinates the bivalent metal ion and also participates in hydrogen bonds in the crystal lattice, whether donor or recipient in these interactions.

In the structure, the units interact through two types of hydrogen bonding: six O – H ... O, being the donor water molecule; and four N – H ... O, being the donor ammonium molecule. Table 5 details these chemical bonds. In either case, the sulfate ion oxygen atoms act as receptors for hydrogen bonds.

The oxygen atoms of the SO_4^{2-} (O1, O2, O3, and O4) are closer to the hydro-

gen atoms of water than to the hydrogens of NH_4^+ . On the other hand, the hydrogen bonding angle is more linear in the former. Therefore, the hydrogen interactions $\text{O}-\text{H}\cdots\text{O}$ is stronger than $\text{N}-\text{H}\cdots\text{O}$. This fact justifies the replacement of the monovalent ion and your non-coordination. Thus the interaction of sulfate in the lattice is more pronounced. But the condition for crystal formation is that the interaction of the ammonium molecule in the lattice also occurs. This fact explains why these crystals exhibit high purity.

Ammonium tetrahedra and cations octahedral surround anions sulfates that have the symmetrical operation of inversion. This arrangement repeats in the stacking of ions along the \bar{a} -axis by translational symmetry. Also, the cations

ammonium stack-up along the \bar{c} -axis.

Water molecules coordinate the metal ion and carry out the packing because it participates in hydrogen bonds between SO_4^{2-} and $[\text{M}(\text{H}_2\text{O})_6]^{2+}$. The six $\text{O}_{\text{water}}-\text{H}\cdots\text{O}_{\text{Sulfate}}$ bonds represent two bonds per water molecule (three crystallographically independent) whose distances of $\text{H}\cdots\text{O}$ interactions range from 1.894(2) to 2.060(3) Å and angles $\text{O}-\text{H}\cdots\text{O}$ of 166(3) to 176(3)°. All atoms of the sulfate ion participate in these moderate interactions, but O1 and O3 act twice as receptors, and O2 and O4 act only once as receivers. In the latter, the interactions are shorter (1.914(2) and 1.894(2) Å, respectively); the interaction values and angles are following table 5.

Only atom O2 does not participate

in $\text{N}-\text{H}\cdots\text{O}$ interactions, while atom O4 is the receptor of two $\text{N}-\text{H}\cdots\text{O}$ interactions. All $\text{N}-\text{H}\cdots\text{O}$ interactions are moderate hydrogen bonds, with $\text{H}\cdots\text{O}_{\text{Sulfate}}$ between 2.019(3) and 2.130(3) Å and $\text{N}-\text{H}\cdots\text{O}_{\text{Sulfate}}$ angles between 158(2) and 179(2)°, according to Table 5.

Raman spectroscopy qualitatively characterized the $\text{M}-\text{O}$ bonds in the octahedral configuration as unchanged. Upon analysis, we realize that the distances between atoms are altered, describing a static occupational disorder modeled by Single-crystal X-ray results. We also characterized $\text{O}\cdots\text{H}$ interactions as sensitive to changes in composition. After analysis, we noticed that most of these bonds are altered, justifying the observations of Raman spectroscopy.

5. Conclusions

The growth model used in the study fits the experimental result, quantified by ICP-OES analysis. There was a deviation in Ni and Co quantities caused by experimental variables resulting from the growth process, but it is possible to adjust for the entire concentration range. The results of Raman spectroscopy concur with predictions of structured group theory and qualitatively model the structure of salts.

From the results, we concluded that the mixed salts crystallize in the space group $\text{P2}_{1/c}$ and point group $2/m(\text{C}_{2h}^5)$,

monoclinic unit cell, presenting two chemical formula units per unit cell ($Z = 2$). The structure is also an octahedron $[\text{M}(\text{H}_2\text{O})_6]^{2+}$ (point group O_h), with $\text{M} = \text{Co}^{2+}$ or Ni^{2+} in the center. Six water molecules occupy your vertices, but only three of them are crystallographically independent. Their point group is C_{2v} , with coordinate molecule properties in the crystal. The octahedrons and tetrahedrons (T_d point group) of SO_4^{2-} and NH_4^+ unite by hydrogen bonds. The crystals have a set of special symmetry positions: a) $\text{E}\{\text{x},\text{y},\text{z}\}$, b) $\text{C}_2\{-\text{x},-\text{y},\text{z}\}$, c) $\text{C}_i\{-\text{x},-\text{y},-\text{z}\}$

and d) $\text{C}_s\{\text{x},\text{y},-\text{z}\}$; and general positions of the group (setting b): a) $\text{E}\{\text{x},\text{y},\text{z}\}$, b) $\text{C}_2\{-\text{x},\text{y}+1/2,-\text{z}+1/2\}$, c) $\text{C}_i\{-\text{x},-\text{y},-\text{z}\}$ and d) $\text{C}_s\{\text{x},-\text{y}+1/2,\text{z}+1/2\}$. M^{2+} atoms attached to water molecules have local symmetry C_i , and the rest of the molecules have local symmetry C_1 .

All analyses contribute cohesively to the structuring of the models, and the mixed salt is isomorphic to the pure salts with structure as the Figure 1. This conclusion can be inferred in the whole concentration range because the mixed salts are isostructural.

Acknowledgments

The authors thank the support of the Crystal Growth Laboratory (DEFIS/UFOP), where the crystals were grown. The Mechanical Testing Laboratory (DEMET/UFOP) by the microscopic

images. The Raman Spectroscopy Laboratory (DEQUI/UFOP) by the Raman analysis. The crystallography Laboratory (DEFIS/UFMG) by the Single-crystal X-ray analysis. The Geochemistry

Laboratory (DEGEO/UFOP) by the ICP-OES analysis. The Coordenação de Aperfeiçoamento de Pessoal de Nível Superior - Brazil (CAPES) - Financing Code 001 by the financial support.

References

- ANDREETA, J. P. *Cristalização: teoria e prática*. São Carlos: IFSC, 1999. 218p.
- ATSARKIN, V. A. Dynamic polarization of nuclei in solid dielectrics. *Sov. Phys. Usp.*, v. 21, n. 9, p. 725-745, 1978.
- BARASHKOV, M. V. ZAZHOGIN, A. A.; KOMYAK, A. I.; SHASHKOV, S. N. Low-Frequency vibrational spectra of tutton salts. *Journal of Applied Spectroscopy*, v. 67, n. 4, p. 445-449, 2000.
- BEST, S. P.; ARMSTRONG, R. S.; BEATTIEB, J. K. Single-crystal Raman Spectroscopy of the α alums $\text{CsM}(\text{SO}_4)_2 \cdot 12\text{H}_2\text{O}$ ($\text{M} = \text{Co}$ or Ir) between 275 and 1200 cm^{-1} . *J. Chem. Soc. Dalton Trans.*, 1992.
- BLEANEY, B.; DANIELS, J. M.; GRACE, M. A.; HALBAN, H.; KURTI, N.; ROBINSON, F. N. H.; SIMON, F. E. Experiments on nuclear orientation at very low temperatures. I. Establishment of a method of nuclear alinement and its application to cobalt-60. *Proc. R. Soc. Lond. A*, v. 221, 1954.
- COTTON, F. A.; DANIELS, J. L. M.; MURILLO, C. A. QUESADA, J. F. Hexaaqua dipositive ions of the first transition series: new and accurate structures; expected and unexpected trends. *Inorg. Chem.*, v. 32, p. 4861-4867, 1993.
- COTTON, F. A.; DANIELS, L. M.; FALVELLO, L. R.; MURILLO, C. A.; SCHULTZ, A. J. Solid solutions of a Jahn-Teller compound in an Undistorted Host. 4. Neutron and X-ray Single-Crystal structures of two Cr/Zn tutton salt solid solutions and the observation of disorder by Low-Temperature neutron diffraction. *Inorg. Chem.*, v. 33, n. 3,

- p. 5396-5403, 1994.
- DONG, J.; LI, X.; ZHAO, L.; XIAO, H.; WANG, F.; GUO, X., ZHANG, Y. Raman observation of the interactions between NH_4^+ , SO_4^{2-} , and H_2O in supersaturated $(\text{NH}_4)_2\text{SO}_4$ droplets. *J. Phys. Chem. B*, v. 111, n. 42, p. 12170-12176, 2007.
- FARRUGIA, L. J. *J. Appl. Crystallogr.*, v. 32, p. 837-838, 1999.
- FEI, S.; STRAWS, H. L. Concerted tunneling in a mixed ammonium (Co, Ni) tutton salt. *J. Phys. Chem.*, v. 99, n. 8, p. 2256-2261, 1995.
- FROST, R. L.; PALMER, S. J.; CEJKA, J.; SEJKORA, J.; PLASIL, J.; JEBAVA, I.; KEEFFE, E. C. A raman spectroscopic study of $\text{M}^{2+}\text{M}^{3+}$ sulfate minerals, romerite $\text{Fe}^{2+}\text{Fe}^{3+}(\text{SO}_4)_4 \cdot 14\text{H}_2\text{O}$ and botryogen $\text{Mg}^{2+}\text{Fe}^{3+}(\text{SO}_4)_2(\text{OH}) \cdot 7\text{H}_2\text{O}$. *J. Raman Spectrosc.*, v. 42, p. 825-830, 2011.
- GANESH, G.; RAMADOSS, A.; KANNAN, P. S.; SUBBIAHPANDI, A. Crystal growth, structural, thermal, and dielectric characterization of Tutton salt $(\text{NH}_4)_2\text{Fe}(\text{SO}_4)_2 \cdot 6\text{H}_2\text{O}$ crystals. *J Therm Anal Calorim.*, v. 112, p. 547-554, 2013.
- GEORGIEV, M.; MARINOVA, D. STOILOVA, D. Vibrational spectroscopy vibrational behavior of matrix-isolated ions in Tutton compounds. III: infrared spectroscopic study of NH_4^+ and SO_4^{2-} ions included in cobalt sulfates and selenates. *Vibrational Spectroscopy*, v. 53, p. 233-238, 2010.
- IVANOVSKI, V.; IVANOVSKI, G. Nearest-neighbour-interaction model in the coupled-optical-phonon-mode theory of the infrared dispersion in monoclinic crystals: application to Tutton salt single crystal. *Spectrochimica Acta Part A*, v. 75, p. 1452-1461, 2010.
- LI, X., LI, Z. Diammonium hexaaquacobalt(II) bis(sulfate). *Acta crystallographica section E*, v. 60, p. 114-115, 2004.
- LIDE, D. R. *et al. CRC Handbook of chemistry and physics*. Boca Raton: CRC Press/Taylor and Francis, 2009.
- LONSDALE, K. Diamagnetic and paramagnetic anisotropy of crystals. *Davy faraday laboratory*, p. 368-389, 1937.
- MARINOVA, D.; GEORGIEV, M.; STOILOVA, D. Vibrational behavior of matrix-isolated ions in Tutton compounds. II. Infrared spectroscopic study of NH_4^+ and SO_4^{2-} ions included in copper sulfates and selenates. *Journal of Molecular Structure*, v. 938, p. 179-184, 2009.
- NAKAMOTO, K. *Infrared and raman spectra of inorganic and coordination compounds*. New York: John Wiley & Sons, 1986.
- PIMPINELLI, A *et al. Physics of crystal growth*. United Kingdom: Cambridge University Press, 1999.
- RAJAGOPAL, P.; ARULDHAS, G. Vibrational Spectra $\text{M}_2\text{Cu}(\text{SO}_4)_2 \cdot 6\text{H}_2\text{O}/\text{D}_2\text{O}$ ($\text{M} = \text{NH}_4$ or K). *Journal of Solid State Chemistry*, v. 80, p. 303-307, 1989.
- REIJERSE, E. J.; VAN DAM, P. J.; KLAASSEN, A. A. K.; HAGEN, W. R.; VAN BENTUM, P. J. M.; SMITH, G. M. Concepts in High-Frequency EPR: applications to Bio-Inorganic Systems. *Appl. Magn. Reson.*, v. 14, p. 153-167, 1998.
- SAITO, Y. *Statistical physics of crystal growth*. Yokohama: World Scientific, 1996.
- SHELDRIK, G. M. Acta Crystallogr., Sect. A: Found. *Crystallogr.*, v. 64, p. 112-122, 2008.
- SHIRRON, P. J.; MCCAMMON, D. Salt pill design and fabrication for adiabatic demagnetization refrigerators. *Cryogenics*, v. 62, p. 163-171, 2014.
- TAHIROV, T. H.; LU, T. A Precise Structure Redetermination of Nickel Ammonium Sulfate Hexahydrate, $\text{Ni}(\text{H}_2\text{O})_6 \cdot 2\text{NH}_4 \cdot 2\text{SO}_4$. *Acta Cryst.*, v. C50, p. 668-669, 1994.
- TELLI, L.; HAMMOUCHE, A.; BRAHIMI, B.; DE DONCKER, R. W. Elaboration of a new anode material for all-solid state Zn/MnO₂ protonic cells. *Journal of Power Sources*, v. 103, p. 201-206, 2002.
- VANDENABEELE, P. *Practical raman spectroscopy: an Introduction*. Chennai: Wiley, 2013.

Received:19 May 2021 - Accepted: 26 September 2022.



All content of the journal, except where identified, is licensed under a Creative Commons attribution-type BY.